A *TRACE* White Light and *RHESSI* Hard X-Ray Study of Flare Energetics

2007 ApJ 656 1187

(http://iopscience.iop.org/0004-637X/656/2/1187)

The Astrophysical Journal, 656:1187–1196, 2007 February 20

A *TRACE* WHITE LIGHT AND *RHESSI* HARD X-RAY STUDY OF FLARE ENERGETICS

L. Fletcher[1]
Department of Physics and Astronomy, University of Glasgow, Glasgow, UK; lyndsay@astro.gla.ac.uk
I. G. Hannah and H. S. Hudson
Space Sciences Laboratory, University of California, Berkeley, CA; hannah@ssl.berkeley.edu, hhudson@ssl.berkeley.edu
and
T. R. Metcalf
NWRA/Colorado Research Associates, Boulder, CO; metcalf@cora.nwra.com
Received 2006 August 15; accepted 2006 October 26

ABSTRACT

In this paper we investigate the formation of the white-light (WL) continuum during solar flares and its relationship to energy deposition by electron beams inferred from hard X-ray emission. We analyze nine flares spanning *GOES* classifications from C4.8 to M9.1, seven of which show clear cospatial *RHESSI* hard X-ray and *TRACE* WL footpoints. We characterize the *TRACE* WL/UV continuum energy under two simplifying assumptions: (1) a blackbody function, or (2) a Paschen-Balmer continuum model. These set limits on the energy in the continuum, which we compare with that provided by flare electrons under the usual collisional thick-target assumptions. We find that the power required by the white-light luminosity enhancement is comparable to the electron beam power required to produce the HXR emission only if the low-energy cutoff to the spectrum is less than 25 keV. The bulk of the energy required to power the white-light flare (WLF) therefore resides at these low energies. Since such low-energy electrons cannot penetrate deep into a collisional thick target, this implies that the continuum enhancement is due to processes occurring at moderate depths in the chromosphere.

Subject headings: X-rays: general — radio continuum: general

Online material: color figures

1. INTRODUCTION

White-light flare emission does not occur only in the most energetic events (the "big flare syndrome"), or in a special class of events. Recent observations show its presence also in weaker events, e.g., down to *GOES* class C7.8 using the *Yohkoh* aspect camera (Matthews et al. 2003), and down to *GOES* class C1.6 using the *TRACE* white-light (WL) channel (Hudson et al. 2006). The modest thermal energies associated with these small flare events point also to modest energy budgets for the nonthermal particles, which are thought to power the WL emission. The model for WL emission is unclear, but the radiation mechanism has generally been attributed to the effects of heating and ionization, producing enhanced Balmer and Paschen contributions as well as the usual H^- continuum. Which continuum dominates depends on the physical conditions in the radiating plasma. The height at which the continuum enhancement occurs is still debated, and ranges from the photosphere itself through the temperature minimum region and the upper chromosphere (Hudson 1972; Aboudarham & Henoux 1986; Ding et al. 2003). Direct excitation of the lower levels would require high-energy electrons: Aboudarham & Henoux (1986) calculate that an electron energy of the order of 100 keV is necessary to reach the lower chromosphere, which places strong demands on the overall flare energetics.

Metcalf et al. (2003) studied the energetics of a large WLF using *TRACE* data and *Yohkoh*/HXT data. They found that there is sufficient energy in the electron beam, provided that the energy for the WLF can come from the lower energy portion of the electron spectrum. Since the low-energy electrons cannot penetrate deep into the atmosphere, Metcalf et al. (2003) concluded that the electron energy is deposited in the upper chromosphere and transported to the deeper layers of the atmosphere via backwarming, primarily in the Balmer and Paschen continua (see also Metcalf et al. 1990a, 1990b). With the much better electron diagnostics available with *RHESSI*, we can improve considerably on the Metcalf et al. (2003) result here.

The bulk of WL flare observations have come from heterogeneous ground-based observations of events scattered over the decades, as summarized by Neidig (1989). The early work suggested striking similarities between WL and HXR emissions (Rust & Hegwer 1975), a phenomenon confirmed by later work (Hudson et al. 1992; Neidig & Kane 1993) including observations from space (Matthews et al. 2003). In the present paper we analyze a set of flares observed by both *TRACE* (Handy et al. 1999) and *RHESSI* (Lin et al. 2002). The data set comes from the *TRACE* WL survey paper of Hudson et al. (2006, hereafter Paper I). That survey generated a complete sample of 11 events above *GOES* C class, based on the requirement that both *TRACE* and *RHESSI* have complete coverage and that *TRACE* provide imaging in its WL and 1700 Å filters at image intervals of 10 s or less. The sample in Paper I extended from *RHESSI* launch (2002 February) through 2004, with the WL flares being observed during a *TRACE* white-light campaign mode. From the end of 2004 to the time of writing no further flares were observed with appropriate *TRACE* coverage. The resulting sample included events with *GOES* classes from C1.6 through M9.1; each event showed clear WL and hard X-ray signals. The WL contrasts ranged from 8% (the C1.6 flare) up to a factor of 4 (the M9.1 flare). These contrast levels are higher than those normally associated with flare WL emission due to the *TRACE* spectral response, which extends to about 1600 Å. Paper I found general consistency with earlier,

[1] Currently visiting researcher, Space Sciences Laboratory, University of California, Berkeley, CA.

TABLE 1
List of *TRACE*/*RHESSI* White-Light Flares Analyzed

Date	Flare Start	Class	Location	*GOES* Peak	WL Peak	HXR Peak	HXR Image Time
2002 Jul 26	18:57	M1.0	S21 E21	19:03	19:01:56	19:02:00	18:59:28 - 19:02:00
2002 Oct 4	05:34	M4.0	S19 W09	05:38	05:36:46	05:35:50	05:35:40 - 05:36:00
2002 Oct 5	10:39	M1.2	S20 W24	10:46	10:41:58	10:42:00	10:41:20 - 10:42:24
2002 Nov 12	17:58	C9.9	S11 W75	18:18	18:16:04	18:16:10	18:15:48 - 18:16:20
2003 Jun 12	01:04	M7.3	N13 W65	01:30	01:23:45	01:26:20	01:23:00 - 01:24:30
2003 Oct 23	02:35	M2.4	N03 E15	02:41	02:39:49	02:39:50	02:39:34 - 02:40:15
2004 Jan 9	01:33	M3.2	N02 E49	01:44	01:40:17	01:40:30	01:39:44 - 01:40:44
2004 Jul 22	00:14	M9.1	N03 E17	00:32	00:30:31	00:30:10	00:29:40 - 00:30:41
2004 Jul 24	13:31	C4.8	N04 W16	13:37	13:34:46	13:34:40	13:34:45 - 13:35:17

mainly ground-based, observations of event morphology but did not deal thoroughly with the energetics of these phenomena. The *TRACE* data, with their high spatial and temporal resolution, showed the WL sources to be intermittent in both space and time.

Of the 11 flares studied in Paper I, two were not included in the present study, as they could not be imaged successfully with *RHESSI*. This was due in one case to insufficient counts (C1.6 on 2004 July 24), and in the other case to missing *RHESSI* aspect-sensor data (C2.7 on 2002 July 25). The flares used in the present study are listed in Table 1, along with the times of their peak flux in *GOES*, 25–50 keV and WL. This table also lists the times for which we carry out *RHESSI* imaging and spectroscopy.

In this paper, we address primarily the energetics of the visible/UV continuum and hard X-rays. *TRACE* WL observations give a measure of the excess energy radiated in the continuum, while with *RHESSI* spectral observations we can calculate the total energy present in the parent electron distribution, under the approximations of the collisional thick-target electron beam model (Brown 1971; Hudson 1972). The main goals of our work are: (1) to examine the spatial relationships between WL and HXRs; (2) to calculate and compare the flare energy budgets implied by the WL and thick-target HXR emissions; and (3) use this to learn about the WL emission mechanism, i.e., above what energy does the parent electron spectrum have enough energy to support the continuum, and what does this energy tell us about the chromospheric height at which the WL emission is formed? Previous recent work in this vein includes studies by Ding et al. (2003) and Chen & Ding (2005, 2006). Ding et al. (2003) combined *Yohkoh* HXT spectra (unfortunately based on only two energy channels) and observations of the infrared Brackett continuum, the development of which was modeled using a flare-excited model atmosphere and radiative transfer based on a four-level plus continuum hydrogen atom. The paper concluded that a beam flux of 10^{10} ergs cm^{-2} s^{-1} was required to explain the continuum enhancement in the 2001 March 10 flare, which could be provided by an electron beam with low-energy cutoff as high as 50 keV. In a further study at Hα + 6 Å and with *RHESSI*, Chen & Ding (2005) conclude that the continuum enhancement in the 2002 September 29 flare requires a low-energy cutoff of 20 keV. In the present paper we adopt the same principle of comparing continuum and HXR to obtain an energy estimate, but extend the study to a larger, consistent sample of flares.

In the following section we give an overview of the *TRACE* WL observations and calculation of the continuum power and in § 3 we examine the spatial relationship between WL and HXR sources. In § 4 we calculate the electron energy flux implied by the collisional thick target, in § 5 we compare this with the energy flux in the visible/UV continuum radiation, and in § 6 we present our discussion and conclusions.

2. *TRACE* RESPONSE AND WL/UV CONTINUUM POWER

The *TRACE* observations that we use cover the visible and UV ranges in two broad spectral bands, and do this with both excellent image resolution and good time cadence. Figure 1 (*left panel*) shows the UV (1700 Å) and WL filter profiles. The excess

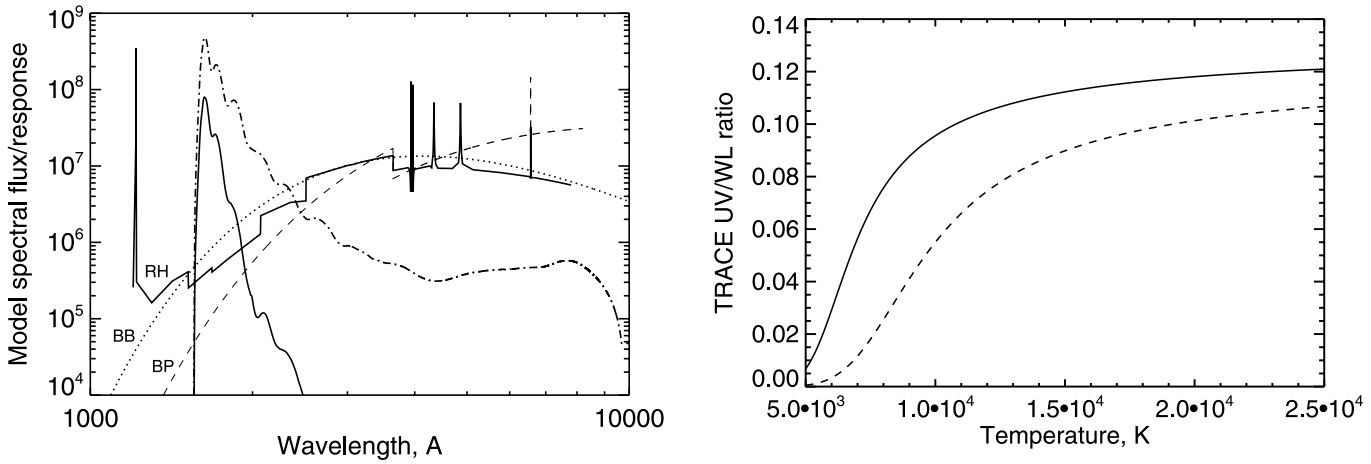

Fig. 1.—*Left*: Model spectra (marked by letters) together with the *TRACE* WL (*dot-dashed line*) and 1700 Å UV (*solid line*) responses as functions of wavelength in Å. The three spectral models are radiative hydrodynamics (RH; see Allred et al. 2005), blackbody (BB; *dotted line*), and Balmer-Paschen (BP; *dashed line*). The latter two models are at 7×10^3 K, a temperature chosen for illustrative purposes only. *Right*: Calculated temperature dependences of the *TRACE* filter ratio (UV/WL) for blackbody (*solid*) and Balmer-Paschen (*dashed*) models.

intensities in each image through a given filter are obtained by subtracting a preflare image in the appropriate spectral band. The ratio of excesses then determines a spectral model with two parameters for the emission in each image pixel, after adjustment for image timing. The exposure times are short, typically a few ms in the WL filter, but the UV images are not simultaneous with them. Thus, for the image characterization we need to assume that the spectrum does not vary with time on scales faster than the image cadence.

To determine the WL/UV energy we need to know its spectral distribution, and there is only limited spectral information in the literature regarding the UV component. This is a persistent problem with observations of WL flares, exacerbated by the extension of the spectrum into wavelengths inaccessible from ground-based observatories. Even at visible wavelengths, there is no systematic knowledge of the continuum spectrum, with few events observed and reported individually. Many of the data were recorded on film; see the early literature as reported by, e.g., Svestka (1976). We note that the strong UV response of the *TRACE* "white-light" channel makes it qualitatively different from all previous observations, largely from ground-based observatories having no sensitivity to the UV. The *Yohkoh* observations, also from space, were in the Fraunhofer G band, and thus more similar to the ground-based data.

Our ignorance of the spectral distribution of the continuum leaves us with several possible choices, as illustrated schematically in Figure 1. The simplest approach is to use the two *TRACE* passbands to define a blackbody spectrum $B_\lambda(T) = 2hc^2/\lambda^5(e^{hc/\lambda kT} - 1)$ with temperature as a parameter. The "Balmer-Paschen model" of Metcalf et al. (2003) is another simple approximation. In this model all of the UV/WL continuum excess spectrum consists of Balmer and Paschen free-bound continua. These continua extend into the UV spectral range, decreasing as exponential functions of the temperature shortward of the Balmer and Paschen edges, respectively. The Balmer-Paschen model was inspired by the "on-the-spot" model for a Stromgren sphere (e.g., Osterbrock 1989), but should be regarded here as a simple ad hoc fitting function. Note that Metcalf et al. (2003) originally defined this approximation without leaving the temperature as a parameter, but using the photospheric value.

The blackbody and Balmer-Paschen models represent two different crude approximations to the complicated physical problems presented by the flaring atmosphere. The next step in sophistication consists of the "radiation hydrodynamics" approach (e.g., Allred et al. 2005, and references therein), which can provide complete spectral information within its simplifying assumptions about the source geometry and dynamics. In our view the uncertainties in this more complete approach currently preclude its direct application to the data at present.

SolarSoft (Freeland & Handy 1998) includes a standard routine `TRACE_UV_RESP` that provides response functions for the two *TRACE* filters used in this analysis, namely the 1700 Å (UV) band and the WL band, as shown in Figure 1 (*left*). This figure also shows three model spectra: a blackbody at 7×10^3 K, the "Balmer-Paschen" model at the same temperature, and one of the radiation hydrodynamics models of Allred et al. (2005). Note the strong rejection of short wavelengths by the *TRACE* filters, notably Lyα. The two *TRACE* passbands overlap because the 1700 Å response consists of the basic WL response plus an additional short-pass filter. The main determinants of the *TRACE* continuum response are the CCD itself, essentially unfiltered for the WL passband, and the Lumogen coating (Handy et al. 1999). This coating converts UV to visible radiation and thus extends the response to short wavelengths.

Figure 2 gives an overview of the WL and HXR light curves of our nine events. The WL light curves represent the excess fluxes in the *TRACE* WL band, integrated over the area at which the UV intensity (*TRACE* 1700 Å band) exceeds 500 DN s^{-1}. We find that this contour includes most of the WL flux. The HXR light curves are the *RHESSI* corrected counts in the 25–50 keV band. Horizontal bars show the times of *RHESSI* attenuator state 1 (thin attenuator in). There were no attenuator movements during the 2002 October 2 and 2002 November 12 flares; in intense flares such as 2003 June 12 and 2004 July 22, the attenuator state alternated between 1 and 3 (thick and thin attenuators in). In the majority of events the WL and HXR peaks correlate well in time; exceptions are discussed later. There appears to be a tendency for the HXR curve to peak slightly ahead of the WL curve. However, because these light curves represent the total fluxes in HXR and WL, and because the WL emission is so intermittent (Hudson et al. 2006), it is probable that the details in the light curves arise in physically different locations.

The UV and WL excess intensities correlate well with one another, at an approximate ratio of 0.2, except possibly for some limited times in two events (2004 July 24 and 2002 October 4) discussed in Paper I. This correlation, plus the fact that the background Sun is so much fainter through the 1700 Å filter, explains why the 500 DN s^{-1} UV contour successfully captures the WL excess.

It is clear that the calculated ratio shown in Figure 1 will not approach the observed value of 0.2, and according to the right-hand panel of Figure 1 the observed *TRACE* spectral ratio (UV/WL) of $\sim$0.2 corresponds to an effective temperature in excess of 2.5×10^4 K in either the blackbody or Balmer-Paschen models. This high temperature should not be taken literally. We speculate that emission lines (pseudocontinuum) may affect the ratio substantially; as Figure 1 shows, a radiation-hydrodynamics spectral model (Allred et al. 2005) can look quite different, and we plan to study this in a subsequent paper. It is also possible that a *TRACE* calibration error explains this high ratio.

Therefore, for the purposes of calculating energetics we can make the following assumptions. Using a photospheric temperature in either blackbody or Balmer-Paschen models will give a lower limit to the WL power, as it ignores the UV component that would result from the elevated temperatures in a flare. An upper limit can be obtained using the temperature value of 2.5×10^4 K in a blackbody model, although until we understand the difference between predicted and observed values of the UV/WL ratio, we anticipate that using this value may greatly overestimate the power.

3. X-RAY FOOTPOINTS AND CORRELATION WITH WHITE LIGHT

We first establish that the hard X-ray and WL flare emission come from the same source location, so that we can directly compare the energy inferred from the two radiation types. Hard X-ray images are reconstructed between 25 and 50 keV using, where possible, the *RHESSI* software implementation of the PIXON reconstruction algorithm (Metcalf et al. 1996). On 2002 July 26 the counts were low, and PIXONs did not resolve the source structure. However, the CLEAN algorithm, which is optimized to break down the image into point sources (but risks overresolving), identified a HXR source with the same shape as the WL sources. It is the CLEAN image that we present for this event. The time intervals over which the images are reconstructed correspond, as nearly as possible, to the peak in the WLF intensity as detected from difference images (or a peak, in the case of more than one significant WL peak), while maximizing also the number

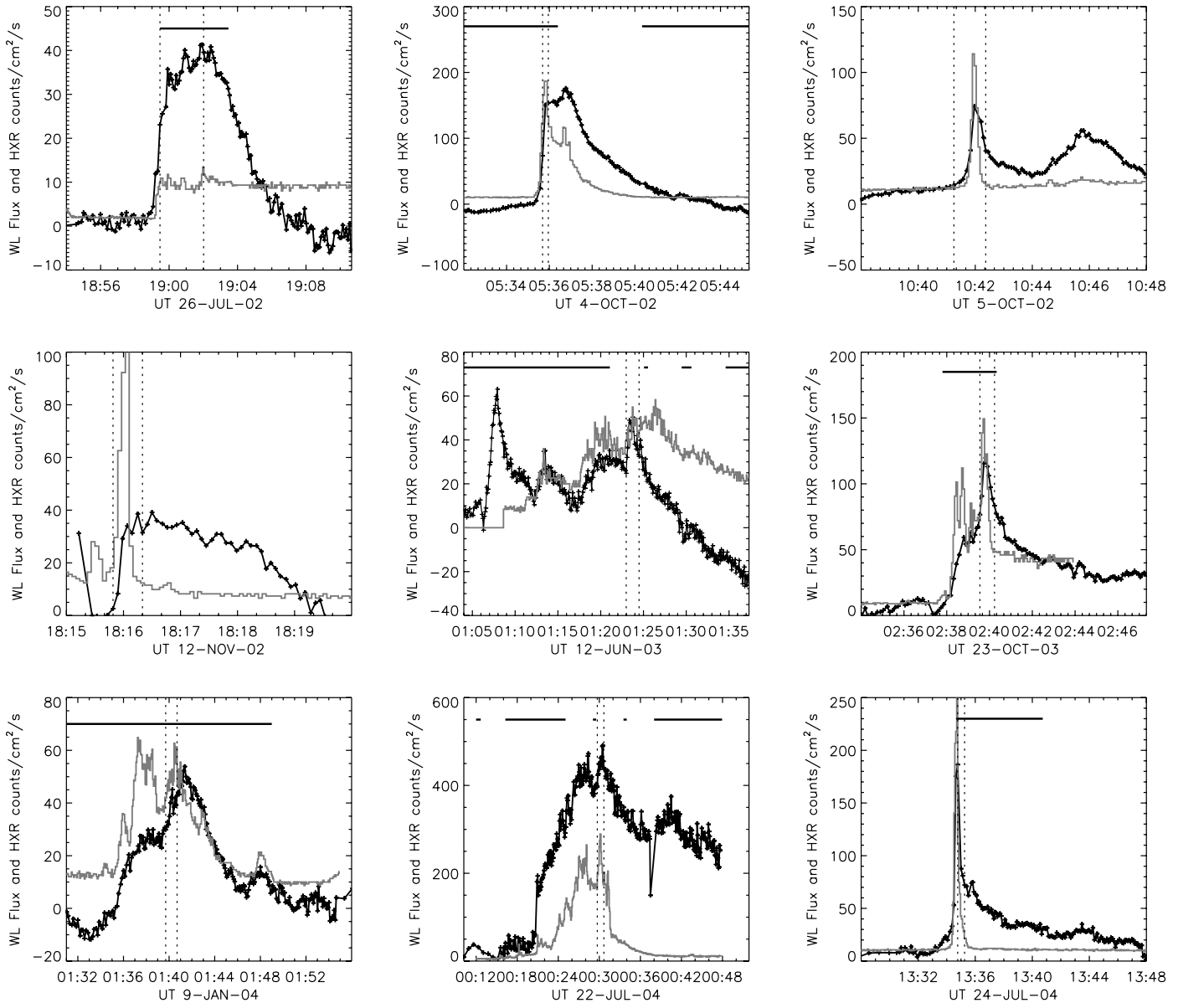

FIG. 2.— Light curves for the nine events as seen in the *TRACE* WL band, obtained by integrating over areas corresponding to the UV contour at 500 DN s^{-1} (*black*), and for the corrected *RHESSI* summary count plots in the interval 25-50 keV (*gray*). *RHESSI* counts have been divided by 3 to fit on the same vertical scale. Vertical lines mark the integration times for the *RHESSI* images and spectra for each event. Also shown by the horizontal bars are the times of *RHESSI* attenuator state 1.

of HXR counts. The time intervals are listed in Table 1. Occasionally, *RHESSI* attenuator movements prevent us from using an imaging interval which includes the WLF intensity maximum, and in this case we use the time interval either just before or just after, whichever has most counts at 25–50 keV. The imaging intervals are at least 20 s long. In the long-lasting event of 2003 June 12 *RHESSI* was in night during the main WL peak at 01:07 UT, and a second peak at 01:24 UT was used.

The *TRACE* pointing is known to drift by up to 10″ over the satellite's orbit, relative to what is reported in the *TRACE* pointing information. However, we can co-align using the white-light images produced by *SOHO*/MDI (Scherrer et al. 1995). Both MDI and *RHESSI* pointing are reliable, *RHESSI*'s extremely so. Therefore, to align *TRACE* WL and *RHESSI* the following procedure was used: a *TRACE* WL image of the active region just before the flare was cross-correlated with the nearest-in-time *SOHO* MDI full-disk white-light image (corrected to Earth view) to establish the offset between *TRACE* WL and MDI. The *TRACE* WL images were then corrected to the MDI reference coordinate system and the MDI WL image and the corrected *TRACE* WL images rotated (using the SolarSoft Mapping software developed by D. Zarro) to the time at which the *RHESSI* image was made, and overlaid. Given the data available, particularly the relatively sparse MDI WL data, there are two unavoidable problems with this process. First, the active region may have evolved between the times of the MDI image and the *TRACE* image used for cross-correlation; second, the solar photospheric rotation model in the Mapping software is an approximation to the actual rotation. Systematic errors will increase with longer time intervals between the MDI WL and flare images. MDI WL images are not made frequently, and in the flares on 2002 October 5, 2002 November 12, 2003 October 23, and 2004 January 9, the lag between the times of the WL flare and the MDI image was more than 1 hr (on the order of 3 hr for the 2002 October 4 and 2004 January 9 events).

A further problem occurs because of the MDI roll angle (angle around the solar line of sight), which must be taken into account

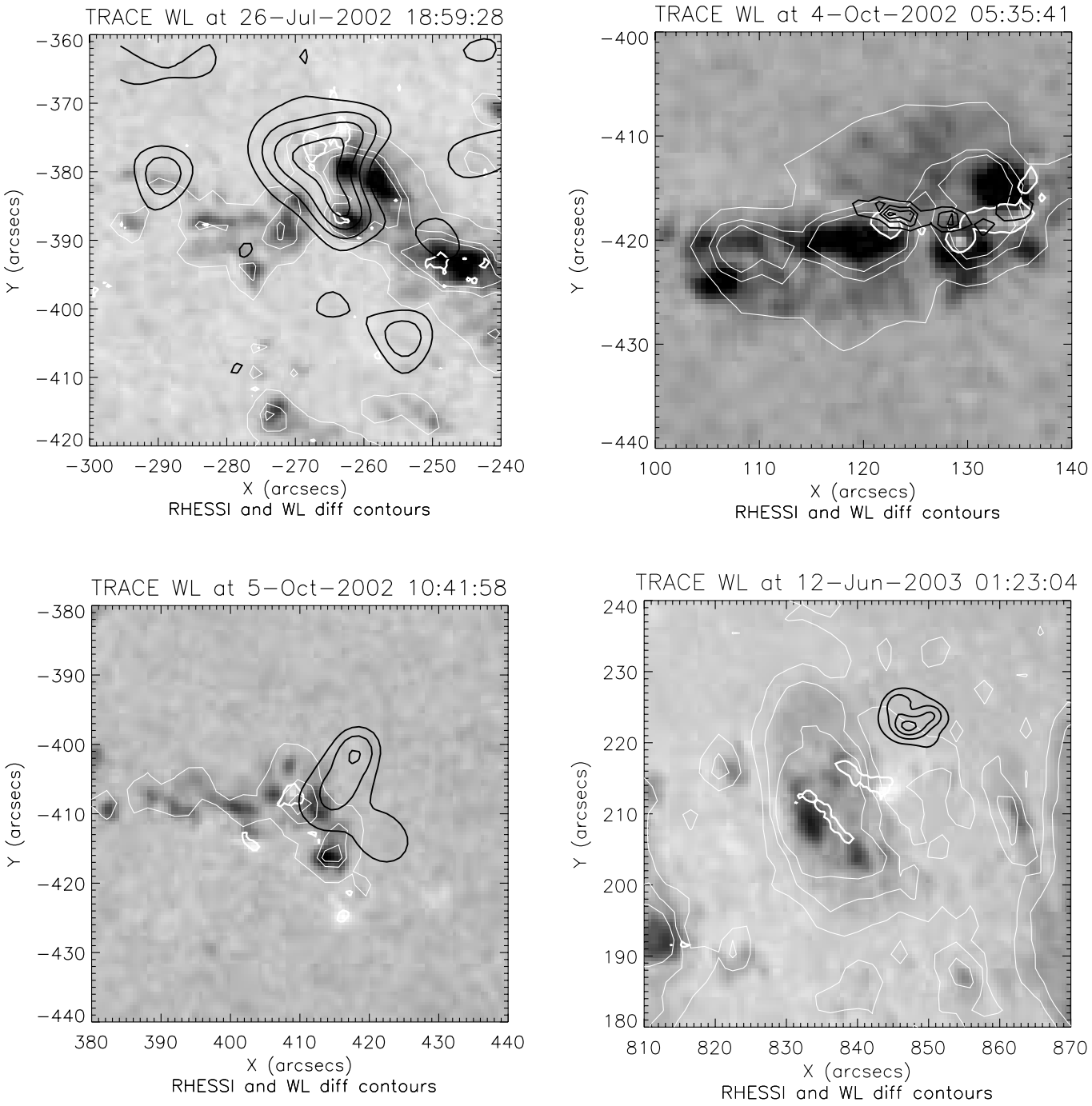

FIG. 3.—Overlays of *RHESSI* hard X-ray (*black*) and WL difference (*thick white*) image contours on a *TRACE* white-light image for four events. The thin white contours show MDI white light; the accuracy of the image cross-correlation and rotation procedure can be assessed by comparing these to the *TRACE* WL background. Offsets between *RHESSI* and *TRACE* WL sources are due to physical offsets in source height, or are a result of the MDI roll, or a combination of the two. [*See the electronic edition of the Journal for a color version of this figure*.]

for precise co-alignments. In the MDI data files, this is reported as being either 0° or 180° (depending on the time of year, since the loss of the *SOHO* high-gain antenna in 2003). However, the difference between the actual roll and these fiducial values averages around 0.22°, varying by several hundredths of a degree (obtained by comparison of MDI and GONG drift-scan observations; J. Schou 2006, private communication). A roll of 0.2° corresponds to a combined *x*-*y* offset of 3″ at the limb. We have proceeded on the assumption that the error in the reported roll angle is zero, but note that including the roll offset effect would always tend to improve the alignment of WL and HXR sources.

In Figures 3 and 4 we show the *TRACE* WL images at the time of maximum *TRACE* WL flare intensity, overlaid with *RHESSI* contours and *TRACE* WL difference contours (showing where the variation of the WL emission is highest). These figures show cases where the predominant emission is from footpoint sources, apart from the 2003 June 12 event (Fig. 3, *bottom left*), where it appears that the HXR source is a coronal source or a displaced footpoint (although it is also not visible in the 1700 Å channel, suggesting a coronal origin). Figure 2 shows that later in this flare the WL and HXR light curves diverge, which may also indicate a different spatial origin. The event of 2002 November 12 in

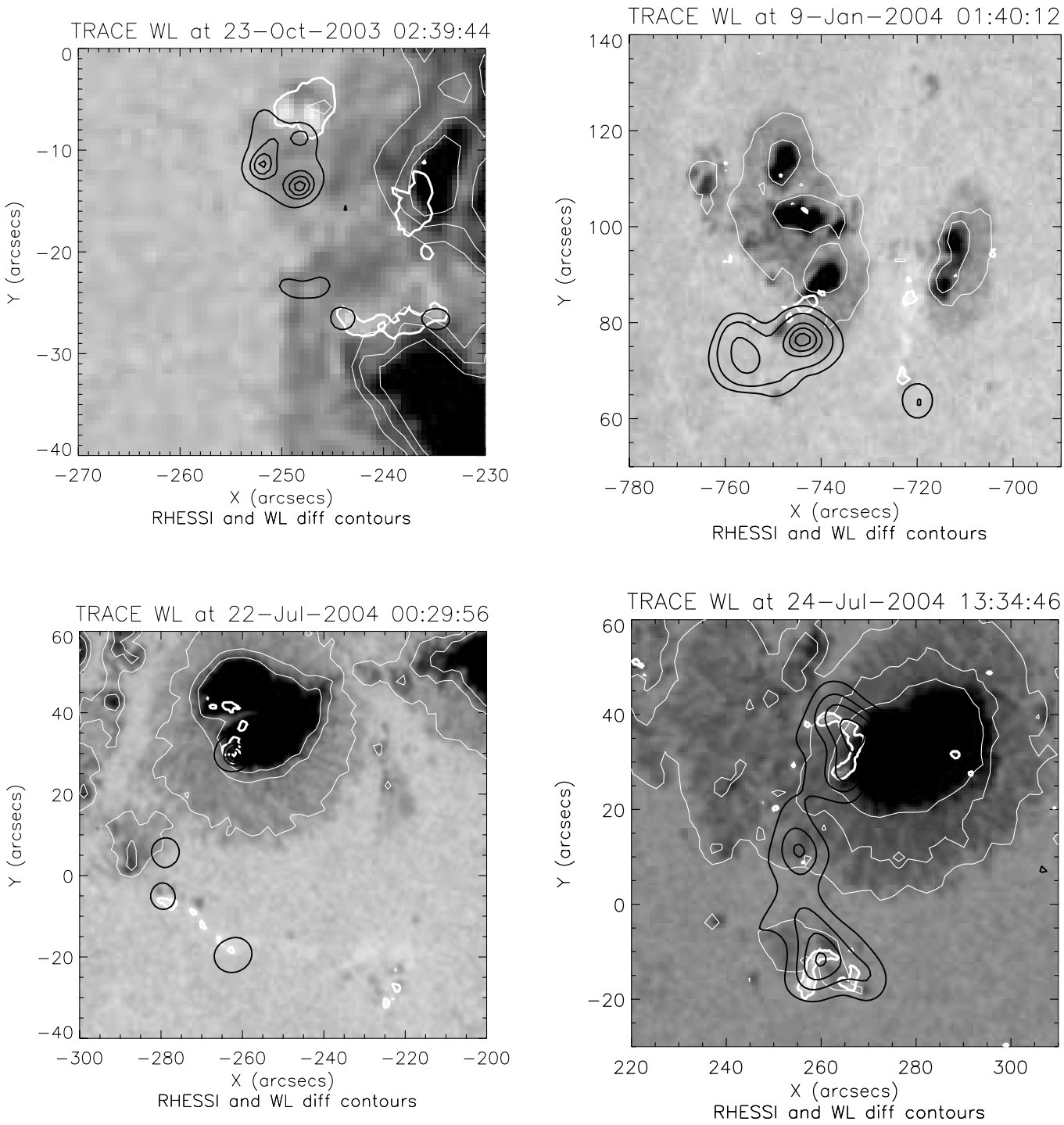

FIG. 4.—Same as Fig. 3, for four more of the event sample. [*See the electronic edition of the Journal for a color version of this figure.*]

Figure 5 shows what appears to be a predominantly coronal HXR source with a faint WL counterpart. In the remaining seven flares the majority of WL and HXR emission appears to come from the chromospheric footpoints. The similarity between the timing of peaks in the WL and HXR light curves of Figure 2 also helps confirm that these sources are at approximately the same location. In some of these, there are noticeable (although usually small) offsets between our HXR and WL images. At this time, we cannot say whether this represents in part a physical offset between the location of the WL and HXR sources (corresponding for example to different depths of formation), or is a result of the uncertainties in coalignment mentioned above. For the time being, if the distribution of WL and HXR sources look similar, but there is a translational offset, then we identify them as the same sources.

4. HXR ENERGETICS

For the times of each of the *RHESSI* images we have analyzed the *RHESSI* photon spectrum. Spectra are modeled with an isothermal component, using the CHIANTI data (Dere et al. 1997; Landi et al. 2006), and a nonthermal component approximated by a broken power law. The isothermal component depends on

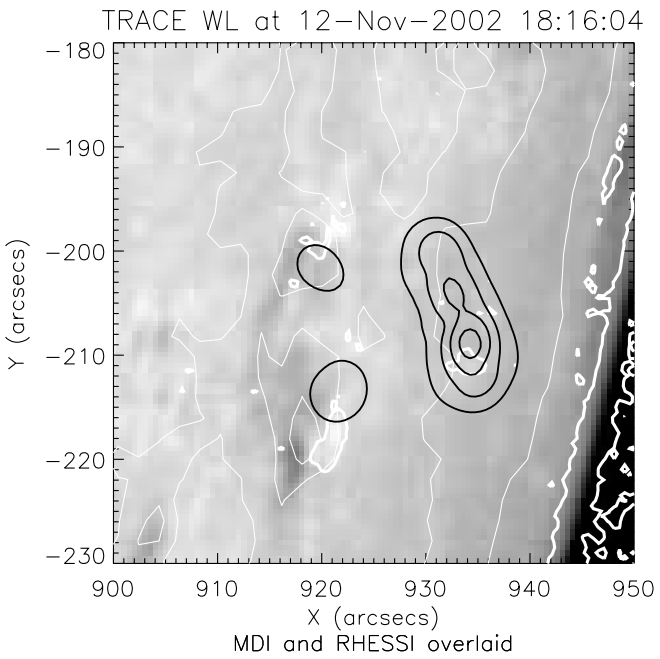

FIG. 5.—Same as Fig. 3, but for the coronal HXR/WL event, 2002 November 12. The *TRACE* 1700 Å images, not shown here, unambiguously identify the large single source with the flare looptops. [*See the electronic edition of the Journal for a color version of this figure.*]

the temperature and emission measure. The broken power law $E^{-\gamma}$ has a fixed index of $\gamma_f = 1.7$ below the break, approximating the expected flattening of the nonthermal photon spectrum in this energy range (e.g., Holman 2003). We have repeated the fits with a low-energy fixed γ_f value of 1.5 and find it makes very little difference to the fit parameters of the high-energy part of the spectrum, since the isothermal component dominates at low energies in any case. Above the break the spectral index is directly related to the index of the assumed power-law electron source distribution. In the 2004 October 4 event a triple power law was required to fit a nonthermal thick-target spectrum to the data.

We have fitted background-subtracted data in the majority of the events, but this was not possible for the two events for which the thick attenuators (Lin et al. 2002) were in place, namely 2003 June 12 and 2004 July 22. These events also show a poor fit of the model at lowest energies, below about 12 keV, which is due to the uncertainty in the instrument response at those energies with the thick attenuators in place. In the other events, where either no attenuator or the thin attenuator is in place, we are confident in the knowledge of the instrumental response down to 6 keV and hence fit above this energy.

The fits are made to a counts spectrum averaged over the imaging interval shown in Table 1. A summary of the fitted photon spectra is shown in Figure 6. Each panel of the figure shows the fit parameters as follows: the temperature of the isothermal component; the volume emission measure; the break energy ϵ_b in the photon spectrum, between the power-law component fitted at high energy, and a low-energy power law with assumed $\gamma_f = 1.7$; the photon spectral index γ above the break; and a normalization constant A_E and the χ^2 goodness-of-fit parameter. The event of 2002 October 4 required a double power law at high energies.

As demonstrated by Brown (1971), it is possible to deduce the instantaneous electron spectrum at injection into the thick target from the fit parameters. As we are dealing with apparently chromospheric sources, the thick target in this case is the chromosphere, and the electron beam powers we will calculate pertain to the beam at the top of the chromosphere. Assuming that the power-law part of the spectrum is generated by electron-proton bremsstrahlung in a collisional thick target, with Bethe-Heitler cross section, the equation for the instantaneous electron power above some energy E_c is then given by

$$P(E \geq E_c) = 5.3\times10^{24}\gamma^2(\gamma-1)B\left(\gamma-\frac{1}{2},\frac{3}{2}\right)AE_c^{1-\gamma}, \quad (1)$$

where B is the beta function, and A is the normalization constant of the photon spectrum $I(\epsilon)$, i.e.

$$I(\epsilon)d\epsilon = A\epsilon^{-\gamma}\,d\epsilon. \quad (2)$$

Similar analyses have been done previously (e.g., Crosby et al. 1993; Lin et al. 2001). We make the refinement of correcting the expression of Lin et al. (2001) for the chromospheric composition via a mean atomic number Z given by $Z^2 = 1.8$.

The parameter A_E returned by the spectral fitting is a normalization constant, and is equal the photon flux at the break energy between high- and low-energy power-law components (indicated by the dotted vertical line in Fig. 6). It can be used to find the normalization constant A for the high-energy power law described by equation (2).

The break energy ϵ_b in the photon spectrum is only an approximation to the low-energy cutoff E_c in the parent electron spectrum; however, it does give a guide. The value of E_c must be greater than ϵ_b, and photons of energy ϵ_b are mostly generated by electrons of energy $\epsilon_b < E < 3\epsilon_b$ (Kosugi et al. 1988). Although the energy of the electron beam extends down to $E = \epsilon_b$, this value is different for each flare, so to be able to compare flares on an equal footing we use two test values of $E_c \geq \epsilon_b$ and calculate the instantaneous beam power carried by electrons above this energy. For the 2002 October 4 event, which is fitted by a three-component model, we adopt the value of γ at intermediate energies ($\gamma = 4.46$), and thus overestimate the power. The values of instantaneous injected beam power obtained are tabulated in Table 2, along with the errors obtained by propagating the errors on the spectral fits through equation (1).

5. VISIBLE/UV CONTINUUM ENERGETICS

In this section we compare the observed UV/WL continuum energy with that inferred from the nonthermal electron beam in the thick-target model. This requires a model assumption, as described above in § 2, that relates the total radiated continuum power to the excess observed in the *TRACE* WL filter.

The energy contained in the visible/UV continuum of a flare cannot precisely be determined by the *TRACE* broadband observations, but we can set a clean lower limit and an approximate upper limit. The lower limit comes from the Balmer-Paschen model of Metcalf et al. (2003) taken at a photospheric effective temperature (5.3×10^3 K), for which a simple formula allows the direct estimate of total radiated energy from the WL excess calculated as described in § 2. We would get larger energies using a temperature closer to the photospheric color temperature of $\sim5.8\times10^3$ K, so this is a conservative assumption in estimating total energy. Using a photospheric temperature certainly gives a solid lower limit, because the continuum energy thus estimated ignores the UV component that would result from increased excitation in the flaring photosphere. Hence, it understates the UV/WL continuum luminosity for a given observed WL flux. A somewhat ambiguous upper limit comes from simply assuming

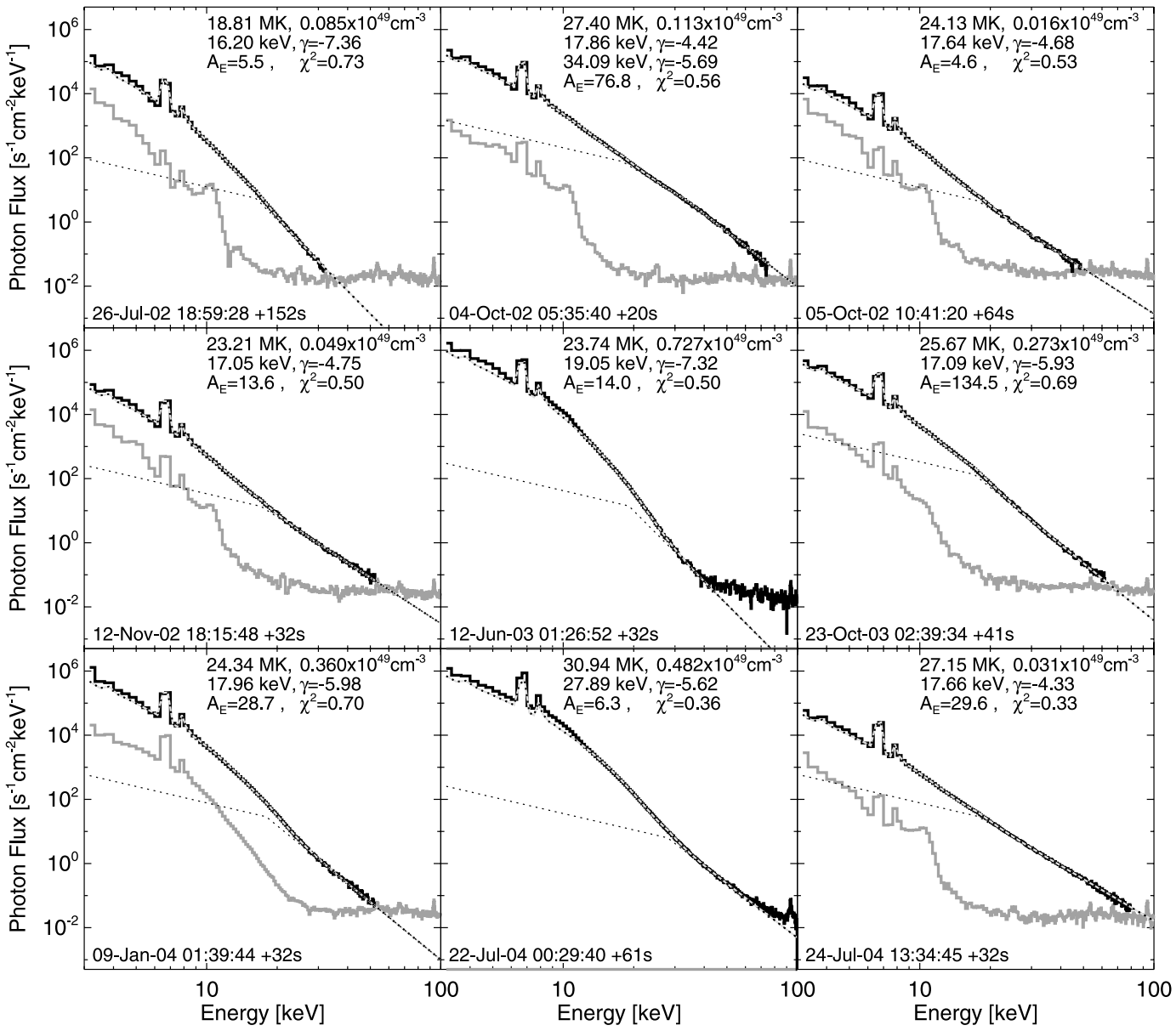

FIG. 6.— Hard X-ray spectra in photon space (*thick black lines*) and their spectral fits (*thick dotted lines*). The background spectra are also shown (*thick gray line*). The spectral model is an isothermal model using CHIANTI, plus a broken power law. The fit parameters are discussed in the text.

TABLE 2

INSTANTANEOUS BEAM POWER AT INJECTION FROM HXR SPECTRAL ANALYSIS

Date	Flare Start	Class	γ	$P \geq 25$ keV (10^{27} ergs s^{-1})	$P \geq 50$ keV (10^{27} ergs s^{-1})
2002 Jul 26	18:57	M1.0	7.4 ± 0.1	0.48 ± 0.05	0.06 ± 0.007
2002 Oct 4	05:34	M4.0	4.42 ± 0.08	16.0 ± 1.4	15.0 ± 1.3
2002 Oct 5	10:39	M1.2	4.667 ± 0.002	0.9 ± 0.001	0.714 ± 0.001
2002 Nov 12	17:58	C9.9	4.75 ± 0.06	2.3 ± 0.2	1.7 ± 0.2
2003 Jun 12	01:04	M7.3	7.30 ± 0.64	5.1 ± 1.1	0.6 ± 0.1
2003 Oct 23	02:35	M2.4	5.93 ± 0.04	21.2 ± 1.8	6.9 ± 0.6
2004 Jan 9.....	01:33	M3.2	6.0 ± 0.1	6.1 ± 1.0	2.7 ± 0.6
2004 Jul 22	00:14	M9.1	5.6 ± 0.1	16.2 ± 1.3	6.6 ± 0.5
2004 Jul 24	13:31	C4.8	4.30 ± 0.03	5.9 ± 0.4	5.8 ± 0.4

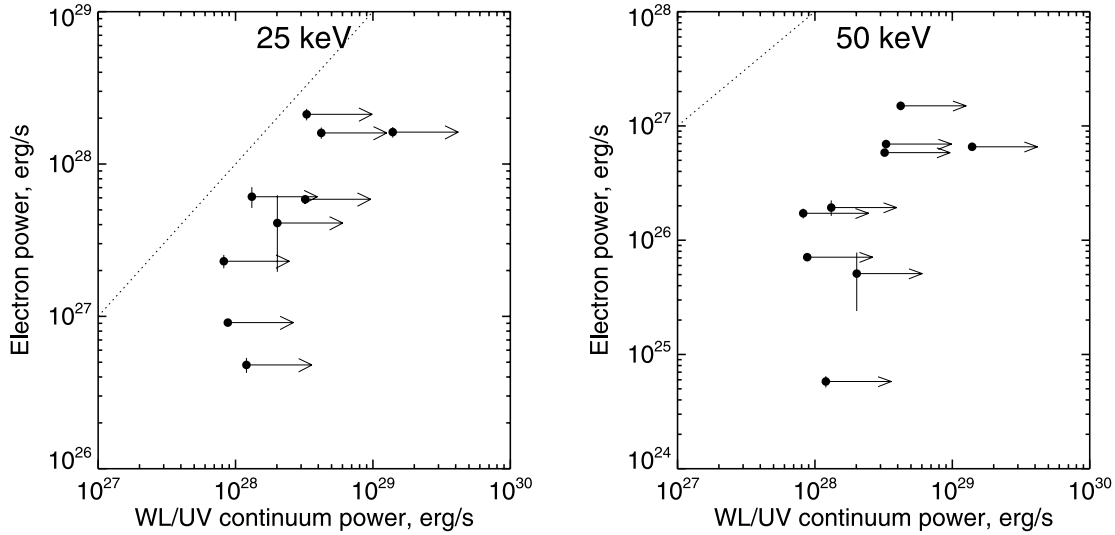

FIG. 7.—Electron energy deposition, based on the thick-target model for low energy cutoffs in the electron spectrum of 25 keV (*left*) and 50 keV (*right*) correlated with visible/UV power (Balmer-Paschen model at photospheric effective temperature, hence lower limits) obtained from the *TRACE* observations. The arrows indicate that all WL/UV continuum power estimates are lower limits, as described in the text. These are mean electron powers over the listed time ranges near the flare peaks. The error bars, visible only for the event of 2003 June 12, show statistical errors for the electron power estimate only; on both axes systematic errors dominate. The dotted lines show equal power levels.

the spectrum to be a blackbody at 2.5×10^4 K. This temperature is consistent with the spectral ratio (UV/WL) we systematically observe in these events; however, we suspect that this blackbody spectral assumption overestimates the UV fluxes and thus also overestimates the radiated energy. Figure 1 shows the spectral distributions of blackbody and Balmer-Paschen models for an intermediate temperature of 7×10^3 K.

These two estimates are a factor $\sim$140 apart; a more precise estimate would require working out the physics of the continuum emission mechanisms in the context of the rapidly evolving source of the radiation. This difficult computational problem is linked inextricably with that of determining the height of formation of the continuum during the flare.

The data allow us to compare flare continuum luminosities (WL plus UV to about 1600 Å) with the electron energy deposition rate inferred from the thick-target model. This is the first time that such a comparison has been made for such a uniform set of data in both the visible-UV continuum and via hard X-rays. Figure 7 and Tables 2 and 3 show the results for our sample of nine flares, with one mean point for each event taken near HXR peak time (as listed in Table 1).

The energy budgets implied by the visible-UV luminosities are larger than those deduced from the collisional thick-target interpretation of the footpoint hard X-rays, even for the lower energy electron beam cutoff energy (25 keV) of our estimates. This is also true for the two events in our sample where the HXRs at 25–50 keV come predominantly from the corona. However, as mentioned in § 4, the cutoff energy could be lower still, with values around the break energy in the electron spectrum (typically $\sim$17 keV). This would increase the electron power by factors between around 4 and 10, sufficient in general to bring the beam power into line with that required by the Balmer-Paschen model at photospheric temperatures. Equivalently, by demanding equality between the two energy budgets, we would arrive at low-energy cutoffs below about 20 keV, corresponding to an electron with range too short to penetrate significantly into the chromosphere. This is true even using the lower limit to the continuum energy provided by the Balmer-Paschen model. The data thus point decisively to lower energy electrons as the source of UV/WL continuum, in the context of the thick-target model, and consequently the source of the UV/WL continuum observed in *TRACE* would be the upper chromosphere.

TABLE 3

TRACE CONTINUUM PARAMETERS AT HXR TIMES

Date	Time	*GOES*	UV Area (10^{18} cm^2)	P1[a] (10^{27} ergs s^{-1})	P2[b] (10^{30} ergs s^{-1})
2002 Jul 26	19:59:28	M1.0	1.87	12	1.7
2002 Oct 4	05:35:41	M4.0	2.99	42	5.9
2002 Oct 5	10:41:58	M1.2	1.74	8.8	1.2
2002 Nov 12	18:15:49	C9.9	3.05	8.3	1.2
2002 Jun 12	01:22:59	M7.3	3.65	23	3.2
2003 Oct 23	02:39:42	M2.4	3.17	33	4.6
2004 Jan 9	01:39:42	M3.2	2.74	13	1.9
2004 Jul 22	00:29:42	M9.1	17.2	140	19.5
2004 Jul 24	13:34:47	C4.8	4.24	32	4.5

[a] Balmer-Paschen power at $T = 5.3\times10^3$ K.
[b] Blackbody power at $T = 2.5\times10^4$ K.

6. DISCUSSION AND CONCLUSIONS

Within the uncertainties associated with overlaying *TRACE* and *RHESSI* images, we have been able to demonstrate in detail that the WL flare emission regions have *RHESSI* hard X-ray counterparts and can be presumed to be footpoints of coronal magnetic loops. Unfortunately, the uncertainties are large enough to prevent us from saying whether there are systematic offsets between the source positions, which may imply formation at different levels in the chromosphere or other discrepancies in our physical model. Offsets between flare HXR and UV sources have been reported previously, for example by Warren & Warshall (2001) using *Yohkoh*/HXT and *TRACE* 1600 Å, and by Alexander & Coyner (2006) using *RHESSI* and *TRACE* 1600 Å. However, the offsets reported by these authors are significantly larger than those we observe and probably correspond to the excitation of different sites in the active region by electron beams with different spectral characteristics (e.g., softer in the regions where there is UV emission but no observable HXR emission). In our case, we believe that the same electron beam is exciting both HXR and WL emission, and it is conceivable that accurate coregistration of the sources could provide information on the relative levels in the atmosphere at which WL and HXR emission is formed.

We have examined the morphology of these flares in terms of their UV/WL spectral ratios, with the finding that a ratio 1:5 describes the *TRACE* filter responses (1700 Å:WL) reasonably well at all times. This finding calls into question the very name "white-light flare," in the sense that the spectrum clearly extends far into the UV. The rarity of the white-light flare phenomenon appears to be a consequence of the much brighter photospheric background at visible wavelengths. The UV component dominates the energetics, but we cannot at present provide quantitative information about this owing to our ignorance of the spectrum.

Finally, we find clear evidence that the visible/UV continuum requires large amounts of energy, large enough to require a cutoff energy in the thick-target model well below 25 keV. Chen & Ding (2006) recently came to a similar conclusion based on comparison of *RHESSI* hard X-ray data and ground-based WL observations of a flare on 2002 September 30. Thus the correlation with ~50 keV X-ray emission noted by Neidig (1989) and others must not properly represent the energetics. There is a discrepancy between the electron range, in the thick-target model, and the large intensity increase at wavelengths corresponding to photospheric or lower chromospheric temperatures that is responsible for the WL flare. The resolution of this issue remains unclear and probably will require further extensive modeling of the flaring atmosphere in the presence of large fluxes of nonthermal particles and radiative backwarming.

We are pleased to acknowledge our anonymous referee, whose comments and insight have clarified and improved this paper. This work was supported by NASA grants NNG05GG17G (L. F. and H. S. H.), NAG5-12878 (T. R. M.), NAS5-98033 (I. G. H. and H. S. H.) and PPARC rolling grant PP/C000234/1 (L. F.). We are grateful to the *RHESSI*, *TRACE* , and *SOHO* teams for their open data policy, which greatly facilitates work such as this. *RHESSI* was built as an international collaboration between University of California at Berkeley Space Sciences Laboratory, NASA Goddard Spaceflight Center and the Paul Scherrer Institute, Switzerland, and is part of the NASA Small Explorer program. *TRACE* is a mission of the Stanford-Lockheed Institute for Space Research (a joint program of the Lockheed-Martin Advanced Technology Center's Solar and Astrophysics Laboratory and Stanford's Solar Observatories Group), and part of the NASA Small Explorer program. MDI is a project of the Stanford-Lockheed Institute for Space Research and is a joint effort of the Solar Oscillations Investigation (SOI) in the W. W. Hansen Experimental Physics Laboratory of Stanford University and the Solar and Astrophysics Laboratory of the Lockheed-Martin Advanced Technology Center. *SOHO* is a project of international cooperation between ESA and NASA.

REFERENCES

Aboudarham, J., & Henoux, J. C. 1986, A&A, 156, 73
Alexander, D., & Coyner, A. J. 2006, ApJ, 640, 505
Allred, J. C., Hawley, S. L., Abbett, W. P., & Carlsson, M. 2005, ApJ, 630, 573
Brown, J. C. 1971, Sol. Phys., 18, 489
Chen, Q. R., & Ding, M. D. 2005, ApJ, 618, 537
———. 2006, ApJ, 641, 1217
Crosby, N. B., Aschwanden, M. J., & Dennis, B. R. 1993, Sol. Phys., 143, 275
Dere, K. P., Landi, E., Mason, H. E., Monsignori Fossi, B. C., & Young, P. R. 1997, A&AS, 125, 149
Ding, M. D., Liu, Y., Yeh, C.-T., & Li, J. P. 2003, A&A, 403, 1151
Freeland, S. L., & Handy, B. N. 1998, Sol. Phys., 182, 497
Handy, B. N., et al. 1999, Sol. Phys., 187, 229
Holman, G. D. 2003, ApJ, 586, 606
Hudson, H. S. 1972, Sol. Phys., 24, 414
Hudson, H. S., Acton, L. W., Hirayama, T., & Uchida, Y. 1992, PASJ, 44, L77
Hudson, H. S., Wolfson, C. J., & Metcalf, T. R. 2006, Sol. Phys., 234, 79
Kosugi, T., Dennis, B. R., & Kai, K. 1988, ApJ, 324, 1118
Landi, E., Del Zanna, G., Young, P. R., Dere, K. P., Mason, H. E., & Landini, M. 2006, ApJS, 162, 261
Lin, R. P., Feffer, P. T., & Schwartz, R. A. 2001, ApJ, 557, L125
Lin, R. P., et al. 2002, Sol. Phys., 210, 3
Matthews, S. A., van Driel-Gesztelyi, L. H. H. S., & Nitta, N. V. 2003, A&A, 409, 1107
Metcalf, T. R., Alexander, D., Hudson, H. S., & Longcope, D. W. 2003, ApJ, 595, 483
Metcalf, T. R., Canfield, R. C., Avrett, E. H., & Metcalf, F. T. 1990a, ApJ, 350, 463
Metcalf, T. R., Canfield, R. C., & Saba, J. L. R. 1990b, ApJ, 365, 391
Metcalf, T. R., Hudson, H. S., Kosugi, T., Puetter, R. C., & Pina, R. K. 1996, ApJ, 466, 585
Neidig, D. F. 1989, Sol. Phys., 121, 261
Neidig, D. F., & Kane, S. R. 1993, Sol. Phys., 143, 201
Osterbrock, D. E. 1989, Astrophysics of Gaseous Nebulae and Active Galactic Nuclei (Mill Valley: Univ. Science Books)
Rust, D. M., & Hegwer, F. 1975, Sol. Phys., 40, 141
Scherrer, P. H., et al. 1995, Sol. Phys., 162, 129
Svestka, Z. 1976, Solar Flares (Dordrecht: Reidel)
Warren, H. P., & Warshall, A. D. 2001, ApJ, 560, L87